Large melting point hysteresis of Ge nanocrystals embedded in SiO_2

Q. Xu,[1,2] I. D. Sharp,[1,2] C. W. Yuan,[1,2] D. O. Yi,[3,2] C. Y. Liao,[1,2] A. M. Glaeser,[1,2] A. M. Minor,[4] J. W. Beeman,[2] M. C. Ridgway,[5] P. Kluth,[5] J. W. Ager III,[2] D. C. Chrzan,[1,2] and E. E. Haller[1,2]

[1]*Department of Materials Science & Engineering, University of California, Berkeley, CA 94720, USA*

[2]*Materials Sciences Division, Lawrence Berkeley National Laboratory, Berkeley, CA 94720, USA*

[3]*Applied Science & Technology, University of California, Berkeley, CA 94720, USA*

[4]*National Center for Electron Microscopy, Lawrence Berkeley National Laboratory, Berkeley, CA 94720,USA*

[5]*Department of Electronic Materials Engineering, Research School of Physical Sciences and Engineering, Australian National University, Canberra ACT 0200, Australia*

(Dated: May 4, 2006)

Abstract

The melting behavior of Ge nanocrystals embedded within SiO_2 is evaluated using *in situ* transmission electron microscopy. The observed melting point hysteresis is large ($\pm 17\%$) and nearly symmetric about the bulk melting point. This hysteresis is modeled successfully using classical nucleation theory without the need to invoke epitaxy.

PACS numbers: 64.60.-i,64.70.Dv,61.46.Hk

The melting/freezing transition is the most familiar of phase transitions and has a long history of quantitative study [1, 2]. The effect of particle size on the melting point (T_m) of crystals has been studied for nearly a century, beginning with the theoretical work of Pawlow [3] and the first experimental observations of Takagi [4]. Thermodynamic analysis [5] predicts that the difference between the bulk and nanocrystal equilibrium melting point should vary as the inverse of the particle radius. This behavior is generally observed for both metallic[6] and semiconductor nanocrystals [7]. Kinetic barriers can cause the observed melting point to differ from the equilibrium value [8], as in the well-known supercooling of small particles [9, 10] and bulk liquids [11]. However, superheating of bulk solids with free surfaces for extended periods of time is thought to be impossible [12]. Here we report that Ge nanocrystals embedded in silica can be both superheated and supercooled by about 17% of the bulk melting point, and we present a classical, continuum thermodynamic theory that explains this behavior.

In crystals of decreasing size, capillarity effects can become prominent. Theories for the thermodynamic equilibrium melting point of free-standing nanocrystals predict that the change in melting point ΔT should scale inversely with radius [6, 8, 13]:

$$\Delta T \propto \frac{T_m}{Lr}\left[\gamma_{L/V}\left(\frac{\rho_S}{\rho_L}\right)^{2/3} - \gamma_{s/V}\right] \tag{1}$$

with r the radius of the nanocrystal, T_m the bulk melting point, L the heat of fusion per volume of the solid phase, and $\rho_L(\rho_S)$ the density of the liquid(solid) phase. For most materials, $\Delta T < 0$, and experimentally it is common to see nanocrystals with $\Delta T = -300$ K.

Experimental observations of melting and freezing, however, are often influenced by the kinetics of the nucleation of the liquid and solid phase, respectively. Lindemann [14] developed the first quantitative mechanism for bulk melting, predicting that melting begins when the amplitude of the vibrational motions in the lattice exceeds a certain threshold value. Surface atoms are less strongly bound, suggesting that melting should begin at the surface, particularly in the case of small particles; this picture is supported by recent molecular dynamics simulations of metal nanocrystals [15]. The phenomena of superheating (an observed T_m above the bulk equilibrium value) and supercooling (an observed T_m below the bulk equilibrium value), are thus intimately tied to the solid/vapor, liquid/vapor and liquid/solid interface energies ($\gamma_{S/V}$, $\gamma_{L/V}$, and $\gamma_{L/S}$, respectively) [12]. If $\gamma_{L/V} < \gamma_{L/S} + \gamma_{S/V}$ a solid phase will not nucleate at the surface, and it may be possible to supercool the liquid phase. In principle, if $\gamma_{S/V} < \gamma_{L/S} + \gamma_{L/V}$ the surface will not premelt and it will be possible to superheat a solid. For bulk materials, the first inequality holds but not the second [12]. Hence, one can often supercool a bulk liquid with free surfaces but not superheat a bulk solid under the same conditions.

For the melting of free-standing nanocrystals, size-dependent kinetic barriers to melting were first considered quantitatively by Couchman and Jesser [8]. They calculated the free energy of a melting particle as a function of the thickness of the molten outer layer. As this layer increases in thickness, the

free energy passes through a maximum, creating a kinetic barrier to melting. The experimentally observed melting point is deduced from the nucleation rate for the transition. Using this treatment, Couchman and Jesser modeled experimental data for several types of nanocrystals that displayed superheating relative to their (depressed) equilibrium melting points predicted by Eq. (1).

Consideration of embedded nanocrystals greatly expands the range of possible behaviors and allows for complete study of the melting point hysteresis. From a classical thermodynamics perspective, there are two major differences between the free-standing and embedded nanocrystal cases. First, the interface energies involved in the melting process differ between the two configurations. In fact, the liquid/vapor and solid/vapor interfaces may no longer be relevant to the melting process, and may be replaced by the liquid/matrix and solid/matrix interface energies. Second, the geometric constraints implied by embedding might lead to different equilibrium and kinetic behaviors.

There are a handful of prior experimental observations of superheating (relative to bulk melting points) of embedded nanocrystals [16–21]. A common feature of most of these studies is the suggestion that interface epitaxy suppresses the vibrational motion of the surface atoms, thus limiting surface premelting and increasing the melting point in accord with the Lindemann criterion. This notion has been incorporated into a phenomenological model for melting [22]. From this perspective, then, it is interesting to consider the melting of nanocrystals confined to an amorphous matrix, as this eliminates the role of epitaxy in any potential superheating [19].

To investigate the effects of confinement in an amorphous matrix on melting, we performed electron diffraction on Ge nanocrystals embedded in silica formed using the process reported earlier [23]. We note that free-standing nanocrystalline Ge has been reported to show the typical melting point depression found for most materials [24].

Electron diffraction was used to study the melting behavior of the embedded nanocrystals. Here the melting temperature is defined as the temperature at which the disappearance of the diffraction pattern occurs, indicating the loss of lattice order. The *in situ* heating and cooling experiments were performed inside a JEOL 3010 transmission electron microscope operating at 300kV. A plan-view specimen was prepared by backthinning the Si substrate and leaving the implanted silica film side untouched. The specimen was then placed in the Gatan Ta628 holder which contains a tantalum furnace and a pair of calibrated thermocouples. The lowest possible electron beam intensity was used to prevent excessive beam heating. Diffraction experiments on Au nanocrystals embedded in SiO_2 were employed to confirm the accuracy of the experimentally measured temperatures. Measurements of their melting point with our experimental approach yielded a melting point in good agreement with expectations, thus validating the experimental technique.

Several heating/cooling cycles were performed in steps of 15 K per 5 minutes from room temperature

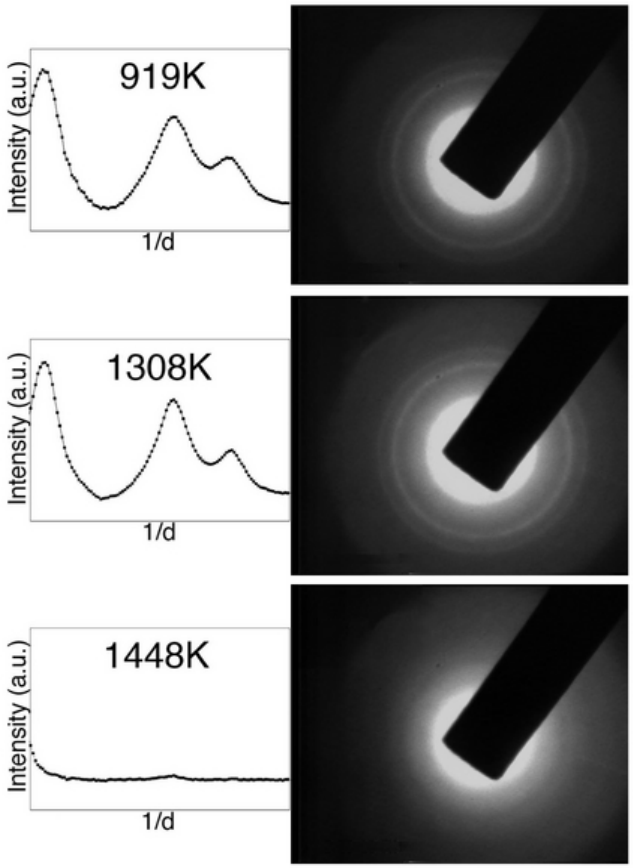

FIG. 1: Diffraction patterns and integrated intensity plots obtained during measurements of the Ge melting point. 1308 K is 97 K above the bulk melting point of Ge; diffraction rings are clearly observed, demonstrating the superheating (relative to the melting point of the bulk) of embedded Ge nanocrystals.

to 1470 K on three Ge nanocrystal specimens. (The nanocrystal coarsening rate was negligible.) All cycles gave identical results. The melting and crystallization were characterized by the intensity change of the diffraction peaks in the selective area diffraction patterns obtained on a 0.2 μm^2 field of embedded nanocrystals. The ring patterns were recorded by a Gatan optically coupled TV-rate CCD camera and integrated circumferentially about the pattern center to produce the reported diffracted intensity.

Electron diffraction patterns obtained while heating Ge nanocrystals in SiO_2 from ambient temperature to 1450 K are shown in Fig 1. The 111, 202, and 113 diffraction peaks persist to 1400 K, nearly 200 K above the bulk melting point (1211 K). Figure 2 displays diffracted intensities (computed by circumferential integration of the patterns shown in Fig. 1) as a function of temperature for heating and cooling cycles, for Ge nanocrystals embedded in silica. Melting starts at 1350 K and is complete by 1450 K; resolidification begins at 980 K and is complete by 880 K. This corresponds to a hysteresis loop approximately 470 K wide and centered (approximately) on the bulk melting temperature.

The observation of a large hysteresis ($\pm$17% of T_m) nearly symmetric about the bulk melting point is

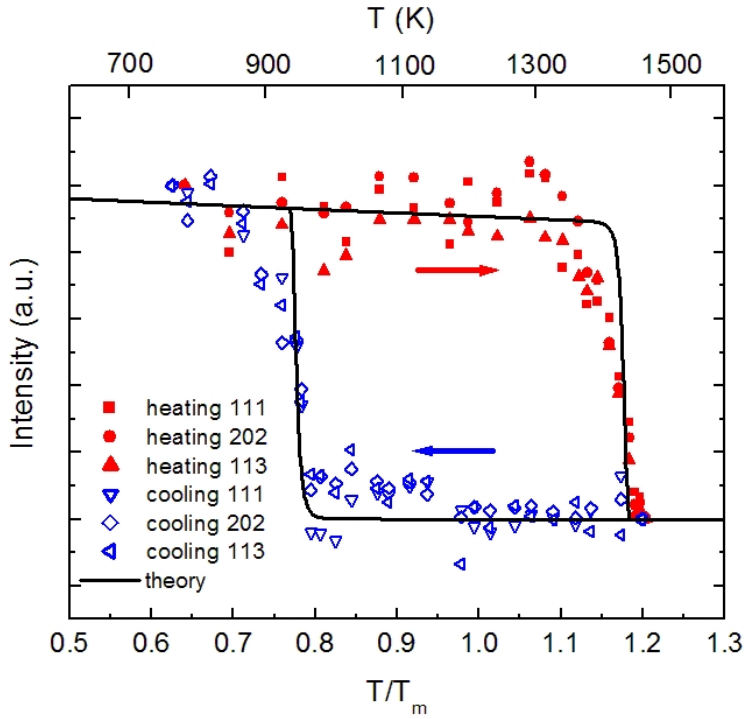

FIG. 2: Intensity of the 111, 202, and 113 Ge diffraction rings as a function of temperature during heating (filled symbols) and cooling (open symbols). Both superheating and supercooling are clearly observed. The solid curve is the prediction of the kinetic theory presented in the text. All temperature measurements are uncertain to ±15 K.

unusual and surprising. The only similar observation of which we are aware is the case of Sn nanocrystals embedded in carbon nanostructures [21]. However, it is demonstrated here that a simple, classical thermodynamics-based model is consistent with all our experimental observations.

There are (at a minimum) two theoretical aspects that need to be addressed in the development of a model for the melting of confined nanoparticles. One must develop a theory for the equilibrium melting point, and one must develop a theory for the kinetics of melting. In developing a kinetic theory, one must construct the proper kinetic pathway. This pathway will be dictated by the geometry of the embedded nanocrystal, and the relevant interface energies.

Determination of the equilibrium melting point requires a model for the change in free energy upon melting. There are three contributions to consider: the change in bulk free energy, the change in interface free energy, and the change in strain energy upon melting. The change in bulk free energies can be related to the latent heat in the standard manner (for T near T_m). The changes in strain and interface energies pose a more formidable theoretical problem.

The density of Ge increases 4.6% upon melting, suggesting that melting may lead to the formation of a gap between the molten droplet and the matrix. However, based on the density change, a 2.5 nm

interface	interface energy (J m^{-2})	notes
$\gamma_{Ge(L)/Ge(S)}$	0.26	Determined from present experiments; close to value in ref. [10].
$\gamma_{Ge(L)/V}$	0.59	Linearly extrapolated from experimental values [25].
$\gamma_{Ge(S)/V}$	1.0	References [26, 27].
$\gamma_{Ge(L)/SiO_2(S)}$	0.91	Reference [25].
$\gamma_{Ge(S)/SiO_2(S)}$	0.91	Determined from present experiments.
$\gamma_{SiO_2(S)/V}$	0.41	Extrapolated from reference [28] data.

TABLE I: Interface energies employed in kinetic model of melting.

radius molten sphere will have an average gap of 0.4 Å between its surface and the matrix (barring the effects of thermal expansion). While this gap is well defined within a continuum theory, its effects at the atomic scale are unclear. Within a continuum theory, the fate of this interface depends upon the values of $\gamma_{Ge(L)/SiO_2(S)}$, $\gamma_{Ge(L)/V}$, and $\gamma_{SiO_2(S)/V}$, and the change in strain energy associated with the suppression or formation of a gap. [Here, (L) indicates liquid, (S) indicates solid and V indicates vapor.] Formation of a gap creates Ge$(L)/V$ and SiO_2/V interface at the expense of Ge(L)/$SiO_2(S)$ interface. Suppression of gap formation puts the liquid Ge in tension, shears the SiO_2 matrix, and might lead to an overall increase in elastic energy. To make further progress, one needs estimates of the interface and strain energies.

The interface energies used on our analysis are given in Table 1. These values, with the exceptions of $\gamma_{Ge(L)/Ge(S)}$ and $\gamma_{Ge(S)/SiO_2(S)}$, are extrapolated from values in the literature or deduced from other experiments independent of the present melting point measurements. Applying the kinetic model described below to description of the experimental data establishes that $\gamma_{Ge(S)/SiO_2(S)} \approx \gamma_{Ge(L)/SiO_2(S)}$, and $\gamma_{Ge(L)/Ge(S)} = 0.26$. This latter value of differs from that quoted by Turnbull [10]. However, Turnbull's analysis employed a calculated heat of fusion, L, that differs from more recent estimates. The melting behavior depends only on the ratio $\gamma_{Ge(L)/Ge(S)}/L$, and scaling Turnbull's value accordingly yields $\gamma_{Ge(L)/Ge(S)} = 0.23$ J/m^2. Our value differs by only 13% - a negligible difference.

The surface energies listed in Table 1 imply the following properties for the embedded nanocrystals. First and foremost, in the solid state, the solid Ge/SiO_2 interface will not premelt because $\gamma_{Ge(L)/SiO_2(S)} + \gamma_{Ge(L)/Ge(S)} > \gamma_{Ge(S)/SiO_2(S)}$. Second, the molten phase will not "presolidify" at the interface because

$\gamma_{Ge(S)/SiO_2(S)} + \gamma_{Ge(L)/Ge(S)} > \gamma_{Ge(L)/SiO_2(S)}$. Thus the solid/liquid transformation will require nucleation in both directions. Third, according to the criteria expressed above, supercooling but not superheating of bulk Ge is predicted, which is consistent with experimental observations.

Based on these interface energies, the opening of a gap would increase the surface energy of a nanocrystal 5 nm in diameter by roughly 70 eV. This increase in surface free energy, would have to be countered through a reduction in strain energy. In the absence of a gap, the liquid would be placed under tension, and be strained roughly 1%. Assuming reasonable values for the bulk modulus of the liquid and the interface stress and applying the formalism in ref. [29], the elastic strain energy is computed to be (roughly) 6 eV. Thus the increase in surface energy associated with opening a gap is roughly an order of magnitude larger than the total strain energy of the liquid phase. In this continuum picture, the elastic energy cannot compensate the increase in interface energy, and a gap will not open. Further, this analysis suggests that elastic contributions are within the accuracy of our theory, negligible.

With these values for the surface energies and neglect of the elastic energy, one can compute two useful quantities for the confined Ge nanocrystals. First, an estimate for the equilibrium melting point can be ascertained. Specifically, we find an expression similar to that of Couchman and Jesser [8] for the change in melting point:

$$\Delta T = \frac{3T_m}{Lr}\left[\gamma_{Ge(L)/SiO_2(S)} - \gamma_{Ge(S)/SiO_2(S)}\right], \tag{2}$$

For our choice of parameters, the term in square brackets is identically zero, as is ΔT.

Second, we can compute an approximate rate for melting and solidification of the confined Ge nanocrystals. The energy barriers are computed by first solving for the equilibrium geometry of the nucleus as a function of liquid volume (using Young's equation and conservation of mass, etc.), and then computing the change in free energy as a function of nucleus size. The maximum in the free energy vs liquid volume plot yields the energy barrier that must be overcome in order to melt or solidify the nanocrystal. Figs. 3(a)-(d) display select configurations along the kinetic pathway. The kinetic theory assumes an attempt frequency per atom of 10^{11} sec^{-1}, that nucleation is heterogeneous at the Ge/SiO2 interface, and that a nucleation rate of 1 sec^{-1} is experimentally observable. Fig. 3(a) is the predicted critical nucleus for the melting of 5 nm diameter nanocrystal and Fig. 3(d) is the critical nucleus associated with solidifying the same nanocrystal. The corresponding predicted superheating and supercooling temperatures are 199 K above and 256 K below the bulk melting point of Ge, respectively. The energy barrier to melting is 3.91 eV, and that associated with solidification is 2.65 eV.

The kinetically determined melting temperatures for the model are plotted in Fig. 3(f). These melting point predictions are then combined with a simple model for diffraction to model the electron diffraction results [30]. Specifically, the diffracted intensity from each nanocyrstal is assumed to scale with the sixth power of the radius, and is corrected for Debye-Waller effects by extrapolating known sub-melting point

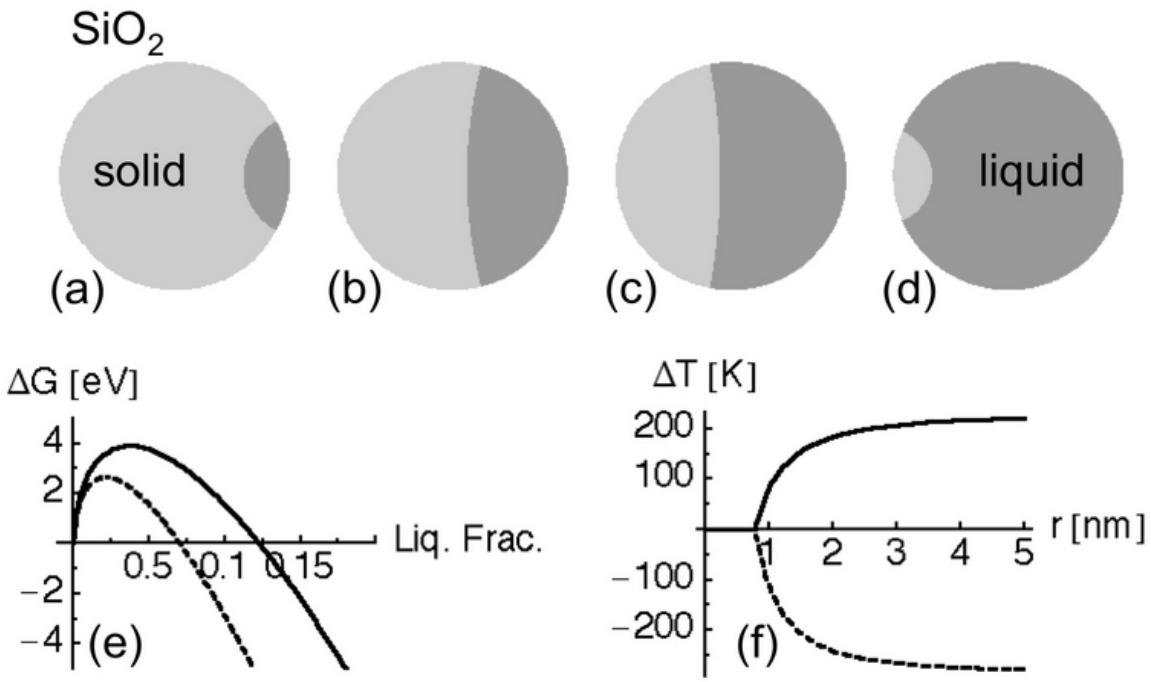

FIG. 3: (a)-(d) The kinetic pathway used to compute the transformation rate. A spherical particle of Ge is embedded in an SiO_2 matrix. The nanocrystal is shown in cross section and is assumed axially symmetric about an axis pointing from left to right. (a) The critical nucleus for melting of an embedded Ge nanocrystal with a 2.5 nm radius at the predicted experimentally observed superheating, 199 K above the bulk melting point. The associated energy barrier is 3.91 eV. (b) and (c) Intermediate configurations along the melting pathway. (d) The critical nucleus for solidification for the same nanocrystal at the predicted supercooling temperature, 255 K below the bulk melting point. The energy barrier to solidification is computed to be 2.65 eV. (e) Free energy curves associated with melting (solid line) and solidfication (dashed line) at the kinetically determined melting points for a nanocrystal with r=2.5 nm. The x-axis represents the fraction of the void that is liquid. (f) The predicted melting (solid) and solidification (dashed) points plotted vs. nanocrystal radius.

behavior [31]. The melting point predictions are convoluted with the measured nanocrystal size distribution [23] and the diffracted intensity from the nanocrystals that are solid at each temperature are reported in Fig. 2. Given the simplicity of the model, the agreement between experiment and theory is excellent.

The model makes clear which surface tensions drive the observed behavior. The change in equilibrium melting point is determined by $\gamma_{Ge(L)/SiO_2(S)} - \gamma_{Ge(S)/SiO_2(S)}$. This quantity also impacts the centering of the hysteresis, as it determines the geometry of the $Ge(S)/Ge(L)/SiO_2(S)$ triple junction. For $\gamma_{Ge(L)/SiO_2(S)} - \gamma_{Ge(S)/SiO_2(S)} = 0$, the contact angle is $\pi/2$, and the hysteresis loop will be nearly symmetric about the bulk melting point. Under these conditions, the width of the hysteresis loop is governed by $\gamma_{Ge(L)/Ge(S)}$. Note that the model also assumes the Ge/SiO_2 interfaces to be smooth. It is possible that the formation

of a very thin Ge-oxide layer between the Ge and SiO_2 might lead to a sufficiently smooth interface.

These experiments demonstrate clearly the advantages of studying embedded nanocrystals. First and foremost, the embedded structure allows for complete study of the melting point hysteresis. Therefore one can assess the relative importance of kinetically limited and equilibrium behaviors directly. Further, the embedded geometry enables the engineering of interface energies and expands substantially the scope of observable melting point behavior.

The authors acknowledge A. Robinson and N. Phillips for their careful reading and insightful critique of this manuscript. I.D.S. acknowledges support from the Intel Robert N. Noyce fellowship. D.O.Y. acknowledges support from U.C. Berkeley and Luce Foundation Fellowships. Q.X. acknowledges support through a U.C. Berkeley Fellowship. D.C.C. and E.E.H. acknowledge support from the Miller Institute for Basic Research in Science. M.C.R. and P.K. acknowledge support from the Australian Research Council. This work is supported in part by the Director, Office of Science, Office of Basic Energy Sciences, Division of Materials Science and Engineering, of the U.S. Department of Energy under contract No. DE-AC02-05CH11231 and in part by U.S. NSF Grant No. DMR-0405472. Electron microscopy was performed at the National Center for Electron Microscopy, LBNL.

[1] R. W. Cahn, Nature **323**, 668 (1986).

[2] R. W. Cahn, Nature **413**, 582 (2001).

[3] P. Pawlow, Z. Phys. Chem. **65**, 1 (1909).

[4] M. Takagi, J. Phys. Soc. Japan **9**, 959 (1954).

[5] K. J. Hansen, Z. Phys. **157**, 523 (1960).

[6] P. Buffat and J.-P. Borel, Physical Review A **13**, 2287 (1976).

[7] A. N. Goldstein, C. M. Echer, and A. P. Alivisatos, Science **256**, 1425 (1992).

[8] P. R. Couchman and W. A. Jesser, Nature **269**, 481 (1977).

[9] D. Turnbull and R. E. Cech, Journal of Applied Physics **21**, 804 (1950).

[10] D. Turnbull, Journal of Applied Physics **21**, 1022 (1950).

[11] A. Defrain, J. Chim. Phys. **74**, 851 (1977).

[12] L. D. Landau and E. M. Lifshitz, *Statistical Physics Part I* (Pergamon Press, Oxford, 1980).

[13] F. Baletto and R. Ferrando, Reviews of Modern Physics **77**, 371 (2005).

[14] F. A. Lindemann, Z. Phys. **11**, 609 (1910).

[15] Y. Qi, T. Cagin, W. L. Johnson, and W. A. Goddard III, J. Chem. Phys. **115**, 385 (2001).

[16] C. J. Rossouw and S. E. Donnelly, Physical Review Letters **55**, 2960 (1985).

[17] J. Dages, H. Gleiter, and J. H. Perepezko, Mat. Res. Soc. Symp. Proc. **57** (1986).

[18] L. Grabaek, J. Bohr, H. H. Andersen, A. Johansen, E. Johnson, L. Sarholt-Kristensen, and I. K. Robinson, Physical Review B **45**, 2628 (1992).

[19] O. S. Mei, S. C. Wang, H. T. Cong, Z. H. Jin, and K. Lu, Physical Review B **70**, 125421 (2004).

[20] Z. Zöllmer, K. Rätzke, F. Faupel, and A. Meyer, Physical Review Letters **90**, 195502 (2003).

[21] F. Banhart, E. Hernández, and M. Terrones, Physical Review Letters **90**, 185502 (2003).

[22] Q. Jiang, Z. Zhang, and J. C. Li, Chem. Phys. Lett. **322**, 549 (2000).

[23] I. D. Sharp, D. O. Yi, C. Y. Liao, J. W. Beeman, Z. Liliental-Weber, K. Yu, D. N. Zakharov, J. W. Ager III, D. C. Chrzan, and E. E. Haller, Applied Physics Letters **86**, 063107 (2005).

[24] N. T. Gladkich, R. Neidermayer, and K. Spiegel, Phys. Stat. Sol. **15**, 181 (1966).

[25] N. Kaiser, A. C. F. R. Szofran, S. D. Cobb, and K. W. Benz, Journal of Crystal Growth **231**, 448 (2001).

[26] M. Albrecht, P. O. Hansen, S. Christiansen, W. Dorsch, H. P. Strunk, and E. Bauser, Scanning Microscopy **8**, 925 (1994).

[27] R. J. Jaccodine, J. Elec. Soc. **110**, 524 (1963).

[28] A. Roder, W. Kob, and K. Binder, J. Chem. Phys. **114**, 7602 (2001).

[29] J. W. Cahn and F. Larche, Acta metallurgica **30**, 51 (1982).

[30] Details will be published elsewhere.

[31] V. F. Sears and S. A. Shelley, Acta Cryst. **A47**, 441 (1991).